

## Guidance of surface waves in a micron-scale phononic crystal line-defect waveguide

Sarah Benchabane, Olivier Gaiffe, Roland Salut, Gwenn Ulliac, Vincent Laude, and Kimmo Kokkonen

Citation: [Applied Physics Letters](#) **106**, 081903 (2015); doi: 10.1063/1.4913532

View online: <http://dx.doi.org/10.1063/1.4913532>

View Table of Contents: <http://scitation.aip.org/content/aip/journal/apl/106/8?ver=pdfcov>

Published by the [AIP Publishing](#)

---

### Articles you may be interested in

[Low-frequency spatial wave manipulation via phononic crystals with relaxed cell symmetry](#)

J. Appl. Phys. **115**, 103502 (2014); 10.1063/1.4867918

[Active wave-guiding of piezoelectric phononic crystals](#)

Appl. Phys. Lett. **99**, 083505 (2011); 10.1063/1.3630231

[Formation of longitudinal wave band structures in one-dimensional phononic crystals](#)

J. Appl. Phys. **109**, 073515 (2011); 10.1063/1.3567911

[Acoustic confinement and waveguiding with a line-defect structure in phononic crystal slabs](#)

J. Appl. Phys. **108**, 084515 (2010); 10.1063/1.3500226

[Scattering of surface acoustic waves by a phononic crystal revealed by heterodyne interferometry](#)

Appl. Phys. Lett. **91**, 083517 (2007); 10.1063/1.2768910

---



**HIDEN**  
ANALYTICAL

## Instruments for Advanced Science

 <p><b>Gas Analysis</b></p> <ul style="list-style-type: none"><li>dynamic measurement of reaction gas streams</li><li>catalysis and thermal analysis</li><li>molecular beam studies</li><li>dissolved species probes</li><li>fermentation, environmental and ecological studies</li></ul>	 <p><b>Surface Science</b></p> <ul style="list-style-type: none"><li>UHV TPD</li><li>SIMS</li><li>end point detection in ion beam etch</li><li>elemental imaging - surface mapping</li></ul>	 <p><b>Plasma Diagnostics</b></p> <ul style="list-style-type: none"><li>plasma source characterization</li><li>etch and deposition process reaction</li><li>kinetic studies</li><li>analysis of neutral and radical species</li></ul>	 <p><b>Vacuum Analysis</b></p> <ul style="list-style-type: none"><li>partial pressure measurement and control of process gases</li><li>reactive sputter process control</li><li>vacuum diagnostics</li><li>vacuum coating process monitoring</li></ul>
--	---	---	---

Contact Hiden Analytical for further details:  
[www.HidenAnalytical.com](http://www.HidenAnalytical.com)  
[info@hiden.co.uk](mailto:info@hiden.co.uk)  
**CLICK TO VIEW** our product catalogue

## Guidance of surface waves in a micron-scale phononic crystal line-defect waveguide

Sarah Benchabane,<sup>1</sup> Olivier Gaiffe,<sup>1</sup> Roland Salut,<sup>1</sup> Gwenn Ulliac,<sup>1</sup> Vincent Laude,<sup>1</sup> and Kimmo Kokkonen<sup>2</sup>

<sup>1</sup>*Institut FEMTO-ST, Université de Franche-Comté, CNRS, ENSMM, UTBM, 15B Avenue des Montboucons, F-25030 Besançon Cedex, France*

<sup>2</sup>*Department of Applied Physics, Aalto University, Tietotie 3, 02150 Espoo, Finland*

(Received 18 November 2014; accepted 13 February 2015; published online 23 February 2015)

We report on the direct observation of trapping and guiding of surface-guided elastic waves in a linear defect introduced into a micron-scale phononic crystal. Elastic field amplitude detection using laser scanning interferometry was used to characterize the different transmission regimes of the one-period wide line defect in a phononic crystal structure as a function of frequency and to discriminate phononic waveguiding from transmission outside the band gap. Surface density-of-states computations support the experimental observations. © 2015 AIP Publishing LLC.

[<http://dx.doi.org/10.1063/1.4913532>]

Phononics is arguably one of the most promising paths towards manipulation and control of acoustic and elastic wave propagation.<sup>1</sup> Phononic crystal cavities and waveguides, for instance, offer the possibility to tailor desirable dispersion properties, potentially leading to dramatically reduced group velocities. Acoustic wave guidance has been predicted<sup>2–5</sup> and shown to occur for bulk<sup>6–10</sup> or Lamb waves<sup>11</sup> in fluid/solid or solid/solid phononic crystals. At the micron-scale, phononic confinement of surface guided waves holds promises for applications in the radio-frequency (RF) regime. Efficient waveguiding solutions would indeed open unexplored routes towards disruptive technologies for the implementation of advanced signal processing functionalities. This particularly holds for surface acoustic wave (SAW) and Lamb-wave based systems that lie at the basis of a number of applications in the fields of wireless telecommunications or micro-electro-mechanical systems (MEMS). Experimental demonstrations of microscale resonators<sup>12,13</sup> and cavities<sup>14</sup> were recently reported. Phononic waveguiding was also lately considered for Lamb waves in phononic crystal slabs<sup>15</sup> and for SAWs in finite-depth phononic crystals.<sup>16</sup>

In this paper, we report on an experimental evidence of surface acoustic wave transmission and confinement in a straight waveguide fabricated into a square-lattice phononic crystal, which we have previously found to feature a phononic band gap (BG).<sup>17</sup> Monochromatic (time-harmonic) surface acoustic waves are generated by a chirped interdigital transducer in order to cover a wide frequency range. The acoustic field amplitude on the sample surface is directly imaged by scanning laser interferometry using the set-up described and used in Refs. 17 and 18. A unique advantage of the interferometric imaging is that each potentially guided wave can be interrogated individually by scanning the input frequency and mapping the induced spatial surface amplitude distribution. The field maps clearly show the existence of several guided modes supported by the one-period wide, or W1, phononic line defect. Guided modes are observed both for frequencies within the phononic band gap and for frequencies falling inside the sound cone for the phononic

crystal. The experimental results are supported by a theoretical analysis of the surface density of states of the fabricated phononic waveguide as a function of frequency and wavevector.

The phononic waveguide was fabricated by introducing a one-period wide line defect in a square-lattice phononic crystal made of air holes milled in an X-cut lithium niobate substrate. The fabrication method applied, along with the experimental results obtained for the defect-free phononic crystal were reported in Ref. 17. The phononic crystal consists of an array of  $8 \times 28$  holes, with a diameter of  $1.9 \mu\text{m}$  and a lattice constant of  $2.1 \mu\text{m}$ . The estimated hole depth is about  $2.5 \mu\text{m}$ . Due to the finite hole depth, radiation losses to the bulk, in particular, for modes lying beyond the sound line, are expected. Surface-guided waves are generated on the sample surface by chirped interdigital transducers designed to deliver a broadband acoustic signal ranging from 630 MHz to over 1.3 GHz. The transducers were fabricated by electron-beam lithography of a Poly(methyl methacrylate) (PMMA) layer followed by a lift-off of a 60-nm thick evaporated aluminum thin film. Their acoustic aperture has been set to  $48 \mu\text{m}$  and is limited by the length of the phononic crystal. SAWs are launched in the direction of the crystallographic Z-axis. A scanning electron microscope (SEM) image of one of the fabricated phononic waveguide devices is shown in Figure 1(a).

The defect-free phononic crystal exhibits a band gap ranging from 650 to 950 MHz, as extracted from both electrical and optical characterizations reported in Ref. 17. Given the waveguide width, we expect to observe a series of guided-modes located within this BG frequency range. It is unlikely, however, that these modes would show up clearly in the RF probe testing of the waveguide sample, since it is expected that the surface-guided modes propagate inside the waveguide and exit it as if originating from a point source located at the waveguide output (see Fig. 1(a)). The resulting cylindrical wave fronts will therefore not match the standard, straight receiving transducer electrode shape, hence preventing signal detection because of electrical interference along each metal finger. Furthermore, we know from previous

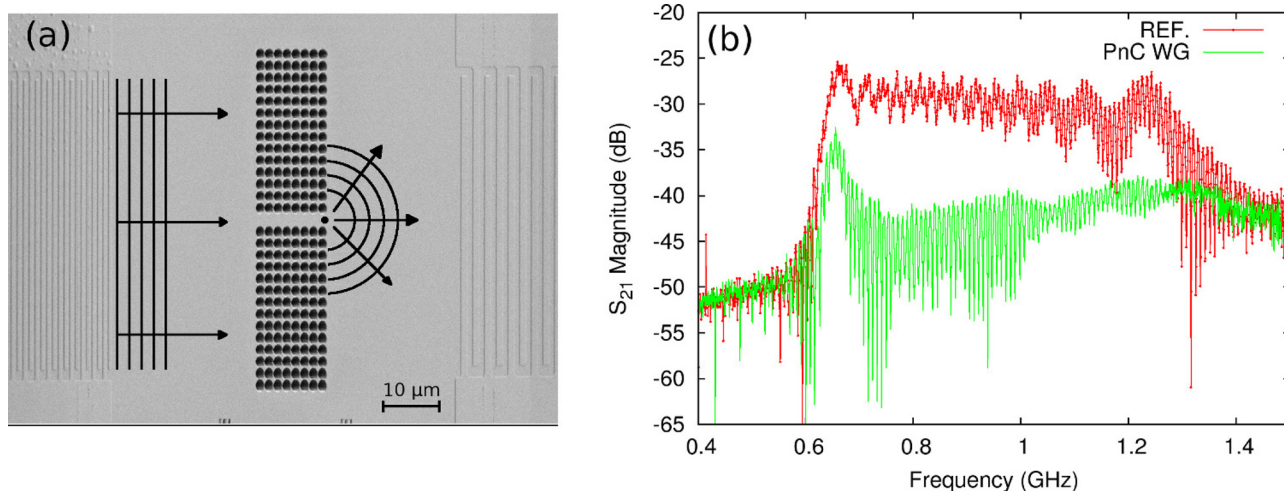


FIG. 1. (a) Scanning electron microscope image of a phononic waveguide device with an eight-period long crystal consisting of a square lattice of air holes etched into lithium niobate. The chirped transducers are visible at the left and right edges of the picture. Schematic drawings of the expected wavefronts launched by the source transducer and leaving the structure after propagation through the waveguide are also shown. (b) Transmission response of the phononic waveguide structure, expressed in terms of  $S_{21}$  scattering parameters, together with the response of a similar structure without a phononic crystal (an electro-acoustic delay line) used as a reference. Note that the receiving transducer is designed to sense SAWs with straight phase fronts and is thus insensitive to the cylindrical SAWs exiting from the waveguide.

experiments with SAW phononic crystals with limited hole depth that surface guided modes located beyond the exit of the band gap remained undetected by the receiving transducer, although their existence was confirmed by wave field measurements using scanning laser interferometry.<sup>17,19</sup> The measured electrical response, displayed in terms of transmission scattering parameters in Figure 1(b), confirms these presumptions. The measurement data are strikingly similar to those observed for the defect-free phononic structure. The entrance of the band gap lies at about 670 MHz, which fits well with the previous sets of measurements. Here again, information provided by RF probe testing is incomplete but it allows us to assess a certain degree of repeatability regarding the phonon source and the band gap position.

The results obtained by scanning laser interferometry shown in Figure 2 are far more instructive. The heterodyne operation allows for a self-calibrated measurement of the absolute amplitude of the out-of-plane component of the surface-guided waves. In an ideal configuration, one would expect the amplitude measurement of a propagating wave to result in a spatially uniform amplitude field signal. The actual case is slightly more complex, however, as several

waves can contribute and interfere at any point of the surface. The amplitude field at the input of the crystal is a combination of plane wave contributions from the piezoelectric source and of reflections at the holes. These latter will lead to strong Bragg reflection within the frequency range of the phononic band gap and to a non-zero signal reflection outside the band gap due to the impedance mismatch induced by the phononic crystal. The amplitude field at the output of the periodical array will be an even more complex combination of partial reflections and transmissions at each hole, of waves bypassing the phononic structure due to its limited width compared to the piezoelectric transducer aperture, and of waves guided within the line defect. This apparently difficult situation actually works in our favor: the presence of several interfering contributions allows us to discriminate the different transmission regimes even in the absence of phase measurements.

In the experiments reported here, the surface waves were generated by applying a RF signal from a signal synthesizer to one of the chirped transducer, while the second one was left unconnected. The out-of-plane amplitude component of the wave field was measured over a wide area,

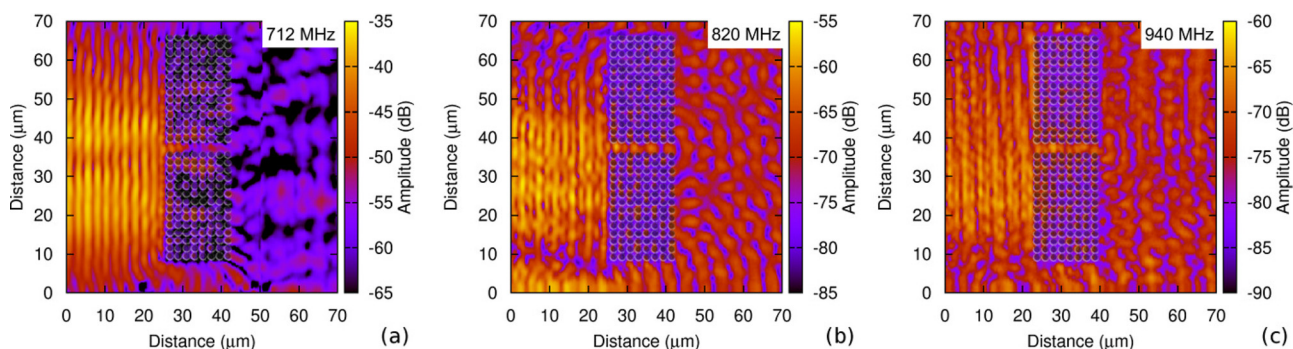


FIG. 2. Measured elastic wave field amplitude maps for excitation frequencies located (a) and (b) inside (712 and 820 MHz) and (c) at the output (940 MHz) of the band gap. The scans cover an area of  $70 \mu\text{m} \times 70 \mu\text{m}$  with an  $0.5 \mu\text{m}$  step size. A semi-transparent scanning electron microscope picture of the holes overlays the measurement data as a guide for the eye. Phonon wave guiding is observed in (b) and (c).

encompassing the whole phononic crystal structure, resulting in  $70\ \mu\text{m} \times 70\ \mu\text{m}$  scans with a  $0.5\ \mu\text{m}$  scanning step. Excitation frequencies were chosen to study wave propagation at frequencies located within as well as below and above the expected phononic band gap frequency range. Figure 2 displays the results obtained at 712 MHz, 820 MHz, and 940 GHz. In all cases, a measurement of the optical reflectivity of the sample is recorded, and the phononic crystal position is superposed on the elastic wave field plots to help localizing the line defect. The emitting transducer is on the left-hand side. The emission angle observed in all cases is about  $4^\circ$  above the Z-axis and corresponds to the natural beam-steering angle for surface acoustic waves propagating in the Z direction on an X-cut lithium niobate crystal.

At 580 MHz, a frequency well below the band gap (see Fig. S1 of the supplementary material), the wave passes through the crystal without being significantly influenced by the periodical array of holes, as expected. The amplitude field at the input is slightly modulated, as a result of the interference between the incoming signal and Fresnel-reflections at the holes. Fig. 2(a) corresponds to a measurement inside the band gap, at 712 MHz. The standing wave pattern at the input is very pronounced and is a characteristic of a very strong Bragg reflection from the phononic crystal. Almost complete signal extinction is observed at the other side of the crystal, confirming the existence of a phononic band gap. SAWs guided by the line defect can be observed in Figs. 2(b) and 2(c). At 820 MHz, a frequency that clearly lies within the band gap, the output field features a very neat interference pattern between a spherical wave issuing from the phononic waveguide and waves bypassing the phononic crystal. No direct contribution of the plane wave source can be observed at the output. The incoming elastic field is transmitted through the waveguide only, resulting in a point-source like emission spot at the output of the line-defect. A standing wave pattern is in addition observed inside the waveguide, probably resulting from the interference of two guided counter-propagating Bloch waves. At 940 MHz, a different transmission mechanism is seen at play. A modulation fringe pattern is still visible inside the waveguide but the free surface at the output now supports ripples rather than highly contrasted fringes. Guidance through the line defect is again observed, that can be attributed to a natural transmission on the plain material compared to the surrounding holey areas. The main contribution at the output is anyway that of a plane wave directly incoming from the source and passing through the crystal. This excitation frequency is indeed located close to the exit of the band gap and consequently some transmission can be expected.

For a more detailed characterization of the wave behavior and to further highlight the difference between the two transmission regimes, detailed scans were carried out, limited to an area of  $60\ \mu\text{m} \times 30\ \mu\text{m}$  centered to the waveguide. Line profiles of the wave amplitude along the line defect were then extracted from these measurements, resulting in the data presented in Figure 3. At 820 MHz, the modulation amplitude of the elastic wave interference pattern is much higher inside the waveguide than at the output of the crystal. This confirms the occurrence of strong interference between Bloch-modes inside the phononic crystal and of a

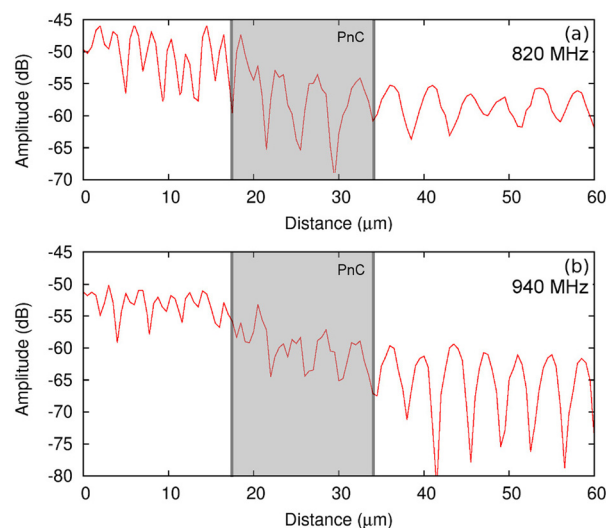


FIG. 3. Amplitude line profiles measured inside the phononic waveguide and along the propagation direction taken at (a) 820 and (b) 940 MHz. The shaded area indicates the position of the phononic crystal (PnC).

predominantly propagating wave at the output. Transmission loss is of the order of 10 dB and includes a significant share of insertion loss due to the modal mismatch between the incident plane wave and the guided mode. At 940 MHz, the modulation strength is much higher at the output of the crystal, clearly indicating an interference phenomenon that involves a plane-wave originating from the emitting transducer that propagates freely through the crystal and a particular contribution travelling through the line defect. The low modulation intensity inside the waveguide corroborates this hypothesis. The transmission at 940 MHz then corresponds to a transmission above the band gap rather than to a transmission through waveguiding. This point is interesting enough on its own as it confirms that waves can propagate even though their dispersion relation stands beyond the sound line. As expected, the transmission is lossy with an output amplitude 15 dB lower than the input signal.

Additional scans, provided as supplementary material,<sup>20</sup> show that wave guidance can be observed at a number of frequencies, particularly in the 800–860 MHz range and at about 750 MHz, though with different guiding strengths. This can point both to several guided modes and to dispersive waveguiding. It has to be noted that our detection technique can underestimate the number of guided modes. Indeed, scanning laser interferometer, like most optical probing techniques, measures only the out-of-plane component of the wave field, therefore missing both in-plane polarized waves or waves that could be polarization-converted at the crystal interface.

To gain further understanding of the phenomena involved, we performed band structure calculations for SAWs in the phononic crystal waveguide. The plane wave expansion (PWE) method,<sup>21</sup> associated to supercell calculations, was used to compute the density of surface states in our phononic crystal waveguide structure in the frequency range centered about the defect-free phononic crystal band gap. 49 harmonics were considered for the computation of the Fourier series. The theoretical model assumes perfectly cylindrical holes instead of the conical holes resulting from

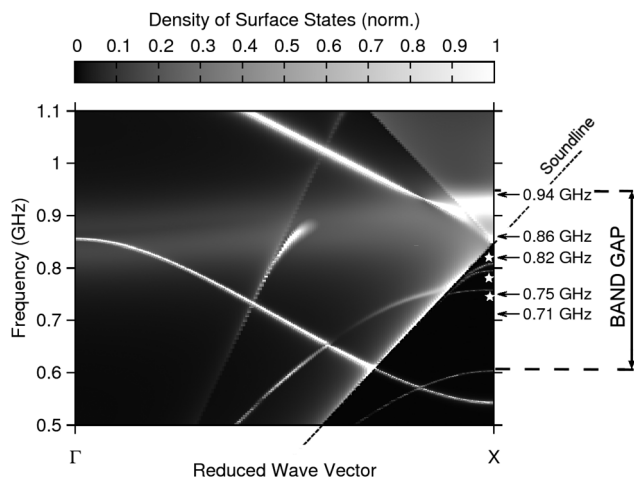


FIG. 4. Density of surface states of radiative and non-radiative surface-guided modes propagating in the  $\Gamma X$  direction for a finite depth phononic waveguide. The computation assumes  $2.5 \mu\text{m}$ -deep and perfectly cylindrical holes. The frequencies displayed on the left-hand side correspond to the excitation frequencies used in the experiments presented in Figs. 2 and 3. The white \* symbols indicate the branches corresponding to the expected guided modes below the sound cone.

FIB milling, but in contrast to our previous work,<sup>21</sup> the finite depth of the phononic crystal is taken into account, hence leading to a more realistic simulation of the actual device. The density of surface states gives us the probability of an elastic mode to be confined to the substrate surface, i.e., it is inversely proportional to the SAW attenuation on propagation. Lossless Rayleigh waves can only be found under the sound cone and leave a bright signature in the band structure plot. Leaky SAW modes inside the sound cone can still be guided by the surface, and high frequency SAW with a dispersion well within the sound cone can actually be observed in the band structure.

The calculated density of surface states presented in Figure 4 is in reasonable agreement with the experiments. A frequency-wise, point-to-point, comparison between experimental and numerical data is not possible, because the limited number of harmonics used for the computation and the conical shape of the holes both cause a frequency-shift of the computed bands. Despite this shortcoming, features corresponding to the experimental observations can be found. The simulations predict several guided waves with flat dispersion, particularly in the upper frequency range of the band gap, which would correspond to the variety of modes experimentally observed between 800 MHz and 860 GHz. Other guided modes can be spotted around 770 MHz, which can roughly correspond to those located at about 750 MHz in the experimental data. The theory also predicts that a reasonable transmission can be expected in the sound cone, in accordance with the experimental observations.

We have demonstrated in this paper the possibility to obtain surface wave guidance and confinement in a micron-scale phononic crystal structure operating in the radio-frequency regime.

A straight waveguide was realized by introducing a missing row of holes in an otherwise perfect square-lattice piezoelectric phononic crystal. The structure was characterized by scanning laser interferometry, enabling direct imaging of the elastic field on the sample and the wave interaction with the phononic crystal structure. The optical measurements clearly confirmed the existence of a bandgap, a result that is in agreement with previous work. Waveguiding was shown to occur for a significant number of frequencies in such a highly multi-mode and dispersive one-period wide waveguide. Additional phase measurements, fabrication of bent waveguides and improvement of the shape of the elastic wave source stand amongst the possible future routes to improve the understanding of surface-wave phononic guidance.

This work has been carried out within Project ANR-09-NANO-004 (phoxcry) funded by l'Agence Nationale de la Recherche (P3N2009) and received a partial support of the French RENATECH network through FEMTO-ST technological facility.

- <sup>1</sup>M. Maldovan, *Nature* **503**, 209 (2013).
- <sup>2</sup>J. H. Sun and T. T. Wu, *Phys. Rev. B* **71**, 174303 (2005).
- <sup>3</sup>L.-Y. Wu and L.-W. Chen, *J. Appl. Phys.* **110**, 114507 (2011).
- <sup>4</sup>V. Laude, J.-C. Beugnot, S. Benchabane, Y. Pennec, B. Djafari-Rouhani, N. Papanikolaou, J. M. Escalante, and A. Martinez, *Opt. Express* **19**, 9690 (2011).
- <sup>5</sup>N. Swintek, S. Bringuier, J.-F. Robillard, J. O. Vasseur, A. C. Hladky-Hennion, K. Runge, and P. A. Deymier, *J. Appl. Phys.* **110**, 074507 (2011).
- <sup>6</sup>A. Khelif, A. Choujaa, S. Benchabane, B. Djafari-Rouhani, and V. Laude, *Appl. Phys. Lett.* **84**, 4400 (2004).
- <sup>7</sup>T. Miyashita, *Meas. Sci. Technol.* **16**, R47 (2005).
- <sup>8</sup>F.-L. Hsiao, A. Khelif, H. Moubchir, A. Choujaa, C.-C. Chen, and V. Laude, *J. Appl. Phys.* **101**, 44903 (2007).
- <sup>9</sup>A. Cicek, O. Adem Kaya, M. Yilmaz, and B. Ulug, *J. Appl. Phys.* **111**, 013522 (2012).
- <sup>10</sup>C. J. Rupp, M. L. Dunn, and K. Maute, *Appl. Phys. Lett.* **96**, 111902 (2010).
- <sup>11</sup>J.-C. Hsu, T.-T. Wu, and H.-S. Hsu, *J. Appl. Phys.* **113**, 083511 (2013).
- <sup>12</sup>S. Mohammadi, A. A. Eftekhari, W. Hunt, and A. Adibi, *Appl. Phys. Lett.* **94**, 051906 (2009).
- <sup>13</sup>N. Wang, F.-L. Hsiao, J. M. Tsai, M. Palaniapan, D.-L. Kwong, and C. Lee, *J. Micromech. Microeng.* **23**, 065030 (2013).
- <sup>14</sup>R. Marchal, O. Boyko, B. Bonello, J. Zhao, L. Belliard, M. Oudich, Y. Pennec, and B. Djafari-Rouhani, *Phys. Rev. B* **86**, 224302 (2012).
- <sup>15</sup>N.-K. Kuo and G. Piazza, in *IEEE International Ultrasonics Symposium* (2010), p. 530.
- <sup>16</sup>P. H. Otsuka, K. Nanri, O. Matsuda, M. Tomoda, D. M. Profunser, I. A. Veres, S. Danworaphong, A. Khelif, S. Benchabane, V. Laude, and O. B. Wright, *Sci. Rep.* **3**, 3351 (2013).
- <sup>17</sup>S. Benchabane, O. Gaiffe, G. Ulliac, R. Salut, Y. Achaoui, and V. Laude, *Appl. Phys. Lett.* **98**, 171908 (2011).
- <sup>18</sup>P. Vairac and B. Cretin, *Opt. Commun.* **132**, 19 (1996).
- <sup>19</sup>K. Kokkonen, M. Kaivola, S. Benchabane, A. Khelif, and V. Laude, *Appl. Phys. Lett.* **91**, 83517 (2007).
- <sup>20</sup>See supplementary material at <http://dx.doi.org/10.1063/1.4913532> for measurements of the out-of-plane amplitude component of the acoustic wave field at additional frequencies.
- <sup>21</sup>V. Laude, M. Wilm, S. Benchabane, and A. Khelif, *Phys. Rev. E* **71**, 036607 (2005).